A Channel Domain Higher-Order SVD Clutter Rejection Filter for Small Vessel Ultrasound Imaging

Kathryn Ozgun and Brett Byram
Department of Biomedical Engineering, Vanderbilt University, Nashville, TN, USA
kathryn.a.ozgun@vanderbilt.edu

***Abstract*—For robust blood flow imaging, filters are used to suppress undesirable noise and clutter signals. In this work, we present a higher-order singular value decomposition (HOSVD) filtering framework. This method is based on a HOSVD applied to a tensor of aperture data, with spatial, slow-time, and channel dimensions. We demonstrate that this HOSVD filtering method can outperform conventional singular value decomposition filters. Preliminary validation of this technique is shown using Field II simulations and *in vivo* data.**

Keywords— Blood flow, power Doppler, higher-order singular value decomposition (HOSVD), singular value decomposition (SVD), clutter rejection.

I. Introduction

Power Doppler imaging, a preferred technique for blood flow visualization, is susceptible to degradation caused by thermal noise and acoustic "clutter" signals, which arise from reverberation, off-axis scattering, and tissue [1], [2]. These sources of degradation particularly impede visualization of small vasculature, as low velocity blood echoes are often close to the noise floor and can exhibit similar temporal characteristics to clutter signals [3].

To improve sensitivity toward blood flow, clutter rejection filters are applied. Conventionally, clutter rejection is achieved using IIR, FIR, or regression filters, which operate along temporal series of Doppler data [3]–[5]. More recently, singular value decomposition (SVD) filters have emerged as a robust alternative to conventional methods. The primary motivation to use SVD filters is that they are inherently adaptive, as the singular vector basis functions are defined by the variance properties of the data. In comparison, conventional filters may be insufficient if complex tissue and blood motion characteristics reside in the same Fourier or polynomial bases. Further, SVD filters can operate on 1-D (temporal) or 2-D (spatiotemporal) data, which expands the feature space for signal classification. As a result, singular value decomposition (SVD) filters can achieve superior performance over conventional methods [1], [6]–[8].

This work was supported in part by the National Institute of Biomedical Imaging and Bioengineering under Grant T32-EB021937, and in part by the National Science Foundation Award under Grant IIS-1750994.
The authors are with the Department of Biomedical Engineering, Vanderbilt University, Nashville, TN 37235 USA (Corresponding author: Kathryn Ozgun, e-mail: kathryn.a.ozgun@vanderbilt.edu).

Higher-order singular value decomposition (HOSVD) filters have recently been proposed to further improve filtering performance [9]. HOSVD has been successfully employed in a multi-rate clutter filtering methodology, initially proposed by Kim et al. [9], [10]. This method has been termed multi-rate because it employs two temporal dimensions: the pulse (slow-time) dimension, which is sampled on the slow-time interval at the pulse repetition frequency, and the Doppler frame dimension, which constitutes a set of pulses. Multi-rate HOSVD has been shown to improve sensitivity toward perfusion in a variety of applications, including for murine [9], [10], tumor [11], and testicular [12] imaging.

However, SVD and multi-rate HOSVD methods of signal separation both predominantly rely on temporal and spatial features. Concurrently, several adaptive beamforming schemes have proposed aperture domain features for clutter mitigation [13]–[16]. This suggests that the aperture data, e.g. delayed channel data, may be leveraged for power Doppler clutter rejection filtering. In addition, several blood flow imaging methods have recently been proposed which rely on clutter rejection operations applied to channel data [17], [18] or sub-aperture data [19], [20], respectively.

We present a clutter rejection filter that uses a HOSVD applied to a tensor of aperture data. We demonstrate that using a multidimensional approach that leverages spatial, slow-time, and channel features can enable greater clutter rejection. Efficacy is shown using simulated and *in vivo* liver data.

II. Background

A. SVD Clutter Rejection Filtering

To perform SVD filtering on Doppler RF data, the depth and lateral spatial extents are often combined in a Casorati form [7]. This produces a 2-D data matrix, $\mathrm{X} \in \mathbb{C}^{M \times N}$ with M spatial samples and N frames. After decomposing the data into its constituent singular value and vector matrices, filtering is performed by weighting or zeroing components that correspond to clutter or noise. The set of components to remove is determined manually or with a classifier that leverages *a priori* assumptions about the data features [6]–[8], [21]. After clutter rejection, the filtered matrix is reconstructed.

B. Higher-Order Singular Value Decomposition

Higher-order singular value decomposition (HOSVD) is the extension of the singular value decomposition to tensors, and a generalization of the Tucker decomposition. The HOSVD of a

978-1-7281-5448-0/20/$31.00 ©2020 IEEE

3-D aperture data tensor, $\boldsymbol{\mathcal{X}} \in \mathbb{C}^{M\times N\times K}$, composed of M spatial samples, N channels, and K frames, is given by

$$\boldsymbol{\mathcal{X}} = \boldsymbol{\mathcal{G}} \times_1 \boldsymbol{U} \times_2 \boldsymbol{V} \times_3 \boldsymbol{W} \tag{1}$$

where $\times_n$ indicates the mode-n product [22]. HOSVD yields a core tensor, $\boldsymbol{\mathcal{G}} \in \mathbb{C}^{M\times N\times K}$, and three unitary matrices: $\boldsymbol{U}$, $\boldsymbol{V}$, and $\boldsymbol{W}$. The unitary matrices are composed of singular vectors, which characterize the dominant features of the data. Our methodology produces singular vectors that correspond to spatial ($\boldsymbol{U}$), temporal ($\boldsymbol{V}$), and channel ($\boldsymbol{W}$) dimensions.

The singular values, which indicate the magnitude of each singular vector, can be computed from the core tensor, $\boldsymbol{\mathcal{G}}$, via a Frobenius norm. For example, the spatial singular values can be computed as

$$\lambda_m^{(1)} = \sum_{n=1}^{N}\sum_{k=1}^{K}\left|\boldsymbol{\mathcal{G}}_{m,n,k}\right|^2. \tag{2}$$

C. Higher-Order Singular Value Decomposition Filter

The HOSVD filtering process is similar to SVD filtering, and is characterized by (1) decomposition of the Doppler data, (2) classification of the dominant signal type contained in each orthogonal component, and (3) rejection of the components corresponding to clutter and noise. We define the HOSVD filter rejection band using four cutoffs, $\{c_{t1}, c_{t2}, c_a, c_s\}$.

Filtering is performed by reducing or zeroing the clutter-dominant components. Therefore, we define the blood core tensor, $\widehat{\boldsymbol{\mathcal{G}}}$, as

$$\widehat{\boldsymbol{\mathcal{G}}}_{m,n,k} = \begin{cases} 0 & for\ \ c_s \le m \le M \\ 0 & for\ \ c_a \le n \le N \\ 0 & for\ \ k \le\ c_{t1}\ and\ \ k \ge c_{t2} \\ \boldsymbol{\mathcal{G}}_{m,n,k} & otherwise \end{cases} \tag{3}$$

and filtered dataset as

$$\widehat{\boldsymbol{\mathcal{X}}} = \widehat{\boldsymbol{\mathcal{G}}} \times_1 \boldsymbol{U} \times_2 \boldsymbol{V} \times_3 \boldsymbol{W}. \tag{4}$$

Finally, the beamsum and power estimation are performed, yielding the power Doppler image, $\mathbf{P_{HOSVD}}$.

III. Methods

Processing and analysis were performed in Matlab (version R2018b, MathWorks, Natick, MA). Beamforming was implemented using the UltraSound ToolBox (v2.1) [23]. The TensorLab (v3.0) function *mlsvd* was used for HOSVD [24].

A. Simulated Data

An 128-element linear probe was designed ($f_0 = 7.81$ MHz, $f_s = 78.13$ MHz) using Field II [25], [26]. Channel data was collected using a plane wave sequence of 13 angles spanning $\pm 2.7°$. Plane wave synthetic focusing (PWSF) was used [27], yielding a net PRF of 700 Hz.

Five 2 x 3 cm tissue phantoms were designed, containing a single 0.4 mm vessel. Blood scatterers were perfused in a parabolic velocity profile, with a maximum velocity of 10 mm/s. Bulk axial motion was applied to the tissue and blood scatterers to simulate realistic clutter. The tissue and blood channel data were simulated separately, and normally distributed random noise was used to simulate electronic noise. The data were combined using a -40 dB blood-to-tissue ratio and a -45 dB noise-to-tissue ratio.

TABLE 1

OPTIMAL PERFORMANCE STUDY CUTOFF RANGES

Parameter	Min	Max	Increment
c_{t1}	1	$K-2$	2
c_{t2}	$c_{t1}+2$	K	2
c_a	8	64	8
c_s	400	1900	300

To assess performance, the HOSVD filter was compared to a SVD filter applied to RF data ($\mathbf{P_{SVD}}$) and to a novel SVD filter applied to the mode-3 unfolded aperture data ($\mathbf{P_{SVD-a}}$), with dimensions of frames $\times$ space*channels.

B. Cutoff Optimization Study

To assess the optimal performance of the filter, a set of power Doppler images were formed by manually defining the HOSVD cutoffs in a bounded grid search over the ranges depicted in Table 1. The reference SVD filters were manually tuned over the c_{t1} and c_{t2} ranges. The filter performance was assessed using measures of contrast, defined as,

$$\text{Contrast} = 10 * log10\left(\frac{\bar{P}_{blood}}{\bar{P}_{backgroud}}\right) \tag{5}$$

and the contrast-to-noise ratio (CNR),

$$\text{CNR} = 10 * log10\left(\frac{\bar{P}_{blood} - \bar{P}_{background}}{\sigma_{background}}\right). \tag{6}$$

In addition, blood flow detectability was measuring using the area under the receiver-operator curve (AUC) as described by Chee et. al [28]. Since the optimal contrast, CNR, and AUC may

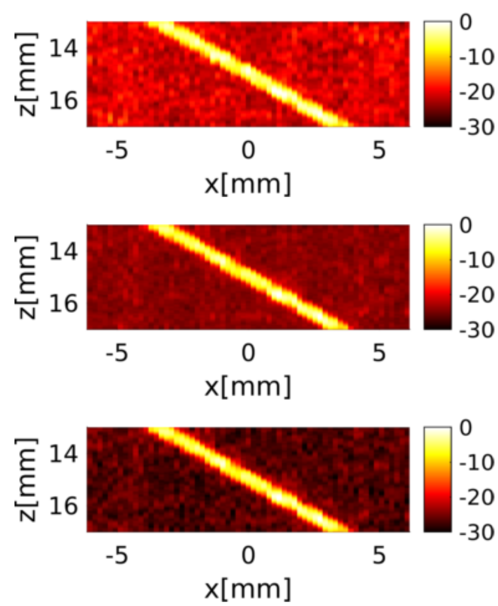

Figure 1. *Top to Bottom:* $\mathbf{P_{SVD}}$, $\mathbf{P_{SVD-a}}$, and $\mathbf{P_{HOSVD}}$ images from the simulation study, shown on a 30dB dynamic range.

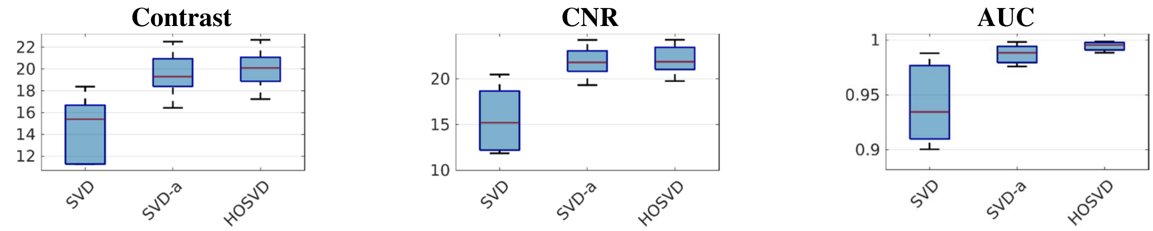

Figure 2. Measures of contrast, contrast-to-noise ratio (CNR), and the area under the curve (AUC) discriminability metric from the simulation study. HOSVD produces greater image quality and discrimination of blood flow. The contrast and CNR are depicted on a dB scale.

correspond to unique cutoff choices, each performance metric was optimized separately. Ensembles of 50 frames were used.

C. In Vivo Data

Liver data was collected from a healthy adult male subject in agreement with local Institutional Review Board (IRB) protocol. Channel data was acquired using a C5-2 probe on a Verasonics research system (Verasonics Inc., Kirkland, WA), with a sequence composed of nine angled plane wave transmits evenly spaced from -4º to 4º. The pulse was designed with a f_0 of 4.167 MHz and f_s of 16.68 MHz. PWSF was applied, producing a net PRF of 600 Hz. Power Doppler images were generated to assess feasibility for clinical imaging applications.

IV. Results

A. Simulated Data

As shown in Figure 2, the HOSVD produced a higher maximum contrast of 19.99 ± 1.97 dB, compared to SVD (14.48 ± 3.13 dB) and SVD-a (19.54 ± 2.21 dB). Similarly, HOSVD produced a higher maximum CNR (22.11 ± 1.72 dB versus 15.59 ± 3.7 dB for SVD and 21.88 ± 1.81 dB for SVD-a). This demonstrates that HOSVD can outperform conventional SVD filtering in an ideal setting.

B. In Vivo Study

In vivo feasibility is demonstrated in liver data, as shown in Figure 3, which depicts the $\mathbf{P_{HOSVD}}$, $\mathbf{P_{SVD}}$, and $\mathbf{P_{SVD-a}}$ images. HOSVD produced greater rejection of clutter and noise, yielding a contrast of 16.20 dB and CNR of 22.72 dB. In comparison, the SVD filter produced a contrast of 14.61 dB and CNR of 20.47 dB, and the SVD-a filter produced a contrast of 15.00 dB and CNR of 21.45 dB. Qualitatively, vasculature is more readily observed with HOSVD filtering in comparison to SVD and SVD-a.

V. Conclusions

We demonstrate a methodology for clutter rejection filtering using a HOSVD filter, which can achieve greater suppression of clutter and noise without loss of blood flow sensitivity. In a future publication, specific features of aperture data will be assessed for the classification of clutter and noise signals.

Acknowledgements

The authors would like to thank the staff of the Vanderbilt University ACCRE computing resource and the contributors to the UltraSound ToolBox.

References

[1] F. W. Mauldin, D. Lin, and J. A. Hossack, “The Singular Value Filter: A General Filter Design Strategy for PCA-Based Signal Separation in Medical Ultrasound Imaging,” *IEEE Trans. Med. Imaging*, vol. 30, no. 11, pp. 1951–1964, Nov. 2011, doi: 10.1109/TMI.2011.2160075.

[2] A. Heimdal and H. Torp, “Ultrasound doppler measurements of low velocity blood flow: limitations due to clutter signals from vibrating muscles,” *IEEE Trans. Ultrason. Ferroelectr. Freq. Control*, vol. 44, no. 4, pp. 873–881, Jul. 1997, doi: 10.1109/58.655202.

[3] S. Bjaerum, H. Torp, and K. Kristoffersen, “Clutter filters adapted to tissue motion in ultrasound color flow imaging,” *IEEE Trans. Ultrason. Ferroelectr. Freq. Control*, vol. 49, no. 6, pp. 693–704, Jun. 2002, doi: 10.1109/TUFFC.2002.1009328.

[4] A. P. Kadi and T. Loupas, “On the performance of regression and step-initialized IIR clutter filters for color Doppler systems in diagnostic medical ultrasound,” *IEEE Trans. Ultrason. Ferroelectr. Freq. Control*, vol. 42, no. 5, pp. 927–937, Sep. 1995, doi: 10.1109/58.464825.

[5] S. Bjaerum, H. Torp, and K. Kristoffersen, “Clutter filter design for ultrasound color flow imaging,” *IEEE Trans. Ultrason. Ferroelectr. Freq. Control*, vol. 49, no. 2, pp. 204–216, 2002.

[6] P. Song, A. Manduca, J. D. Trzasko, and S. Chen, “Ultrasound Small Vessel Imaging With Block-Wise Adaptive Local Clutter Filtering,” *IEEE Trans. Med. Imaging*, vol. 36, no. 1, pp. 251–262, Jan. 2017, doi: 10.1109/TMI.2016.2605819.

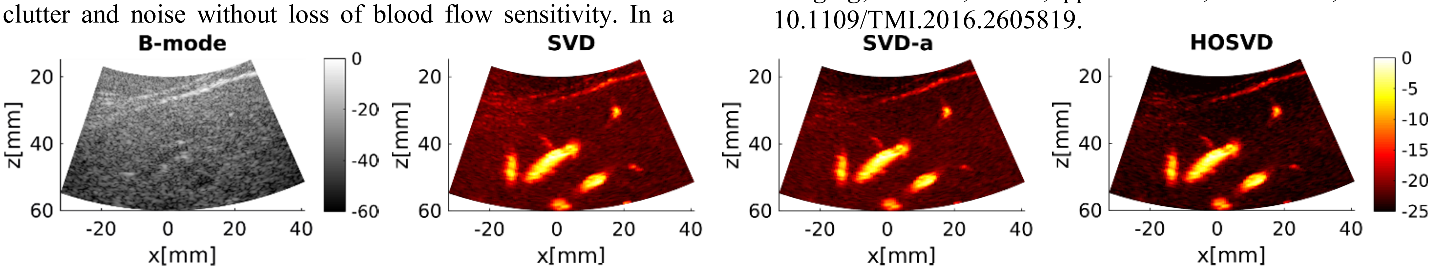

Figure 3. *L*eft to Right*:* B-mode, $\mathbf{P_{SVD}}$, $\mathbf{P_{SVD-a}}$, and $\mathbf{P_{HOSVD}}$ images from the liver study.

[7] C. Demene *et al.*, "Spatiotemporal Clutter Filtering of Ultrafast Ultrasound Data Highly Increases Doppler and fUltrasound Sensitivity," *IEEE Trans. Med. Imaging*, vol. 34, no. 11, pp. 2271–2285, Nov. 2015, doi: 10.1109/TMI.2015.2428634.

[8] J. Baranger, B. Arnal, F. Perren, O. Baud, M. Tanter, and C. Demene, "Adaptive Spatiotemporal SVD Clutter Filtering for Ultrafast Doppler Imaging Using Similarity of Spatial Singular Vectors," *IEEE Trans. Med. Imaging*, vol. 37, no. 7, pp. 1574–1586, Jul. 2018, doi: 10.1109/TMI.2018.2789499.

[9] M. Kim, C. K. Abbey, J. Hedhli, L. W. Dobrucki, and M. F. Insana, "Expanding Acquisition and Clutter Filter Dimensions for Improved Perfusion Sensitivity," *IEEE Trans. Ultrason. Ferroelectr. Freq. Control*, vol. 64, no. 10, pp. 1429–1438, Oct. 2017, doi: 10.1109/TUFFC.2017.2719942.

[10] M. Kim, Y. Zhu, J. Hedhli, L. W. Dobrucki, and M. F. Insana, "Multidimensional Clutter Filter Optimization for Ultrasonic Perfusion Imaging," *IEEE Trans. Ultrason. Ferroelectr. Freq. Control*, vol. 65, no. 11, pp. 2020–2029, Nov. 2018, doi: 10.1109/TUFFC.2018.2868441.

[11] M. Bayat, A. Alizad, and M. Fatemi, "Multi-rate higher order singular value decomposition for enhanced non-contrast ultrasound Doppler imaging of slow flow," in *2018 IEEE 15th International Symposium on Biomedical Imaging (ISBI 2018)*, Apr. 2018, pp. 1178–1181, doi: 10.1109/ISBI.2018.8363781.

[12] G. G. Olleros, C. A. Villagómez Hoyos, K. L. Hansen, M. B. Stuart, and J. A. Jensen, "Spatiotemporal Filtering for Synthetic Aperture Slow Flow Imaging," in *2018 IEEE International Ultrasonics Symposium (IUS)*, Oct. 2018, pp. 1–4, doi: 10.1109/ULTSYM.2018.8579611.

[13] M. A. Lediju, G. E. Trahey, B. C. Byram, and J. J. Dahl, "Short-lag spatial coherence of backscattered echoes: imaging characteristics," *IEEE Trans. Ultrason. Ferroelectr. Freq. Control*, vol. 58, no. 7, pp. 1377–1388, Jul. 2011, doi: 10.1109/TUFFC.2011.1957.

[14] J. Camacho, M. Parrilla, and C. Fritsch, "Phase Coherence Imaging," *IEEE Trans. Ultrason. Ferroelectr. Freq. Control*, vol. 56, no. 5, pp. 958–974, May 2009, doi: 10.1109/TUFFC.2009.1128.

[15] Pai-Chi Li and Meng-Lin Li, "Adaptive imaging using the generalized coherence factor," *IEEE Trans. Ultrason. Ferroelectr. Freq. Control*, vol. 50, no. 2, pp. 128–141, Feb. 2003, doi: 10.1109/TUFFC.2003.1182117.

[16] M. K. Jeong and S. J. Kwon, "Estimation of side lobes in ultrasound imaging systems," *Biomed. Eng. Lett.*, vol. 5, no. 3, pp. 229–239, Sep. 2015, doi: 10.1007/s13534-015-0194-y.

[17] Y. L. Li and J. J. Dahl, "Coherent flow power doppler (CFPD): flow detection using spatial coherence beamforming," *IEEE Trans. Ultrason. Ferroelectr. Freq. Control*, vol. 62, no. 6, pp. 1022–1035, Jun. 2015, doi: 10.1109/TUFFC.2014.006793.

[18] K. Ozgun, J. Tierney, and B. Byram, "A Spatial Coherence Beamformer Design for Power Doppler Imaging," *IEEE Trans. Med. Imaging*, pp. 1–1, 2019, doi: 10.1109/TMI.2019.2953657.

[19] C. H. Leow *et al.*, "3-D Microvascular Imaging Using High Frame Rate Ultrasound and ASAP Without Contrast Agents: Development and Initial In Vivo Evaluation on Nontumor and Tumor Models," *IEEE Trans. Ultrason. Ferroelectr. Freq. Control*, vol. 66, no. 5, pp. 939–948, May 2019, doi: 10.1109/TUFFC.2019.2906434.

[20] A. Stanziola, C. H. Leow, E. Bazigou, P. D. Weinberg, and M.-X. Tang, "ASAP: Super-Contrast Vasculature Imaging Using Coherence Analysis and High Frame-Rate Contrast Enhanced Ultrasound," *IEEE Trans. Med. Imaging*, vol. 37, no. 8, pp. 1847–1856, Aug. 2018, doi: 10.1109/TMI.2018.2798158.

[21] A. Yu and L. Lovstakken, "Eigen-based clutter filter design for ultrasound color flow imaging: a review," *IEEE Trans. Ultrason. Ferroelectr. Freq. Control*, vol. 57, no. 5, pp. 1096–1111, May 2010, doi: 10.1109/TUFFC.2010.1521.

[22] L. De Lathauwer, B. De Moor, and J. Vandewalle, "A Multilinear Singular Value Decomposition," *SIAM J. Matrix Anal. Appl.*, vol. 21, no. 4, pp. 1253–1278, Jan. 2000, doi: 10.1137/S0895479896305696.

[23] A. Rodriguez-Molares *et al.*, "The UltraSound ToolBox," in *2017 IEEE International Ultrasonics Symposium (IUS)*, Washington, DC, Sep. 2017, pp. 1–4, doi: 10.1109/ULTSYM.2017.8092389.

[24] Vervliet N., Debals O., Sorber L., Van Barel M. and De Lathauwer L., "Tensorlab | A Matlab package for tensor computations." https://www.tensorlab.net/ (accessed Apr. 23, 2020).

[25] J. A. Jensen and N. B. Svendsen, "Calculation of pressure fields from arbitrarily shaped, apodized, and excited ultrasound transducers," *IEEE Trans. Ultrason. Ferroelectr. Freq. Control*, vol. 39, no. 2, pp. 262–267, Mar. 1992, doi: 10.1109/58.139123.

[26] J. A. Jensen, "FIELD: A Program for Simulating Ultrasound Systems," in *10th Nordicbaltic Conference on Biomedical Imaging, Vol. 4, Supplement 1, Part 1:351–353*, 1996, pp. 351–353.

[27] G. Montaldo, M. Tanter, J. Bercoff, N. Benech, and M. Fink, "Coherent plane-wave compounding for very high frame rate ultrasonography and transient elastography," *IEEE Trans. Ultrason. Ferroelectr. Freq. Control*, vol. 56, no. 3, pp. 489–506, 2009.

[28] A. J. Y. Chee and A. C. H. Yu, "Receiver-Operating Characteristic Analysis of Eigen-Based Clutter Filters for Ultrasound Color Flow Imaging," *IEEE Trans. Ultrason. Ferroelectr. Freq. Control*, vol. 65, no. 3, pp. 390–399, Mar. 2018, doi: 10.1109/TUFFC.2017.2784183.